CHEMISTRY OF MATERIALS
Cite This: Chem. Mater. 2018, 30, 3454−3466
Article
pubs.acs.org/cm

Non-Invasive Characterization of the Organic Coating of Biocompatible Quantum Dots Using Nuclear Magnetic Resonance Spectroscopy

Chengqi Zhang,[†] Goutam Palui,[†,§] Birong Zeng,[†,‡] Naiqian Zhan,[†,∥] Banghao Chen,[†] and Hedi Mattoussi*[,†]

[†]Department of Chemistry and Biochemistry, Florida State University, Tallahassee, Florida 32306, United States
[‡]Department of Materials Science and Engineering, Fujian Provincial Key Laboratory of Fire Retardant Materials, Xiamen University, Xiamen, Fujian 361005, China

Supporting Information

ABSTRACT: Colloidal quantum dots, made of semiconductor cores and surface coated with an organic shell, have generated much interest in areas ranging from spectroscopy to charge and energy transfer interactions to device design, and as probes in biology. Despite the remarkable progress in the growth of these materials, rather limited information about the molecular arrangements of the organic coating is available. Here, several nuclear magnetic resonance (NMR) spectroscopic techniques have been combined to characterize the surface ligand structure(s) on biocompatible CdSe-ZnS quantum dots (QDs). These materials have been prepared via a photoinduced ligand exchange method in which the native hydrophobic coating is substituted, in situ, with a series of polyethylene glycol-modified lipoic acid-based ligands. We first combined diffusion ordered spectroscopy with heteronuclear single-quantum coherence measurements to outline the conditions under which the detected proton signals emanate from only surface-bound ligands and identify changes in the proton shifts between free and QD-bound ligands in the sample. Quantification of the ligand density on different size QDs was implemented by comparing the sharp ^{1}H signature(s) of lateral groups in the ligands (e.g., the OCH_3 group) to an external standard. We found that both the molecular architecture of the ligand and the surface curvature of the QDs combined play important roles in the surface coverage. Given the non-invasive nature of NMR as an analytical technique, the extracted information about the ligand arrangements on the QD surfaces in hydrophilic media will be highly valuable; it has great implications for the use of QDs in targeting and bioconjugation, cellular imaging, and energy and charge transfer interactions.

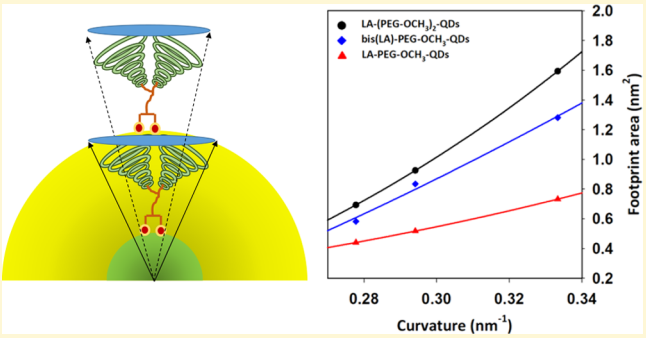

INTRODUCTION

Colloidal quantum dots are crystalline nanomaterials with size-, composition-, and shape-tunable optical and electronic properties.[1−4] They exhibit unique photophysical properties, including broad absorption spectra with large extinction coefficients, narrow and symmetric emission profiles, and remarkable photostability and chemical stability. They have generated great scientific interest over the past three decades, for use in many energy-related and biorelated areas, e.g., photovoltaic and other optoelectronic devices, biosensing, and *in vivo* tissue imaging.[5−17] Apart from these inherent properties, they possess another important characteristic: their surface coating is often complex and affects several of their photophysical properties.[16,18−21] The coating is made of organic ligands/surfactant molecules that coordinate on the nanocrystal cores, while promoting interactions with the immediate environment; this provides steric stabilization to the nanocrystals in solution phase. The nature of the ligand coordination, its density, and its lateral extension play an important role in controlling the nanocrystal properties, e.g., hydrodynamic size, effective charge, long-term colloidal stability, and biocompatibility. The ligand arrangement on the nanocrystals is also highly relevant for controlled conjugation of the nanocrystals to target biomolecules. Therefore, a thorough understanding of the ligand arrangement on the nanocrystals is essential for optimizing the material's performance in biological as well as nonbiological matrices.

High-quality quantum dots (QDs, e.g., CdSe-ZnS core−shell nanocrystals), grown via "hot injection" methods, are the most promising nanomaterial for developing fluorescent platforms that can be effectively integrated with biological systems.[9,22−25] As synthesized, the QDs are coated with a set of hydrophobic ligands. Interfacing them with biological systems thus requires postsynthetic surface modification. Several methods, often

Received: March 9, 2018
Revised: April 25, 2018
Published: April 26, 2018

DOI: 10.1021/acs.chemmater.8b01033
Chem. Mater. 2018, 30, 3454−3466

involving ligand exchange with coordinating molecules or encapsulation within amphiphilic coatings, have been developed to prepare water compatible QDs.[26−34] A wide range of coordinating ligands containing anchors such as carboxyls, amines, imidazoles, and pyridines have been recently tested.[31,35−40] However, because of the strong metal coordination of thiol groups to Zn- and Cd-rich surfaces, the use of dihydrolipoic acid-modified monomers, oligomers, and polymers combined with ligand exchange has successfully been applied by several groups.[38,41−52] Despite the continuous efforts geared toward ligand design and the preparation of functional biocompatible QD surfaces, a thorough characterization of the capping layer on hydrophilic QDs is still lacking; this reflects the difficulty of such a task and the complexity of these inorganic/organic hybrid nanomaterials.

Various analytical techniques, including thermogravimetric analysis (TGA), X-ray photoelectron spectroscopy (XPS), gel permeation chromatography (GPC), and matrix-assisted laser desorption ionization time-of-flight (MALDI-TOF) and inductively coupled plasma mass spectrometry (ICPMS), have been used to characterize the surfaces of various nanoparticles.[22,53−61] While these techniques have yielded useful information about the coating layer, they have encountered a few stringent limitations. For instance, characterizing only surface-coordinated ligands without interference from those unbound in the sample is rather difficult; similarly, preserving the integrity of the nanoparticle surface coating during sample preparation and purification is tedious. Nuclear magnetic resonance (NMR) spectroscopy has recently emerged as one of the most promising techniques for characterizing the structure and dynamics of the organic coating of colloidal nanomaterials. Because it is nondisruptive, NMR can simultaneously probe combinations of surface-coordinated ligands, under various conditions, without altering the integrity of the nanoparticle−coat complex. ^{1}H NMR and ^{13}C NMR combined with ^{31}P NMR have been used to characterize the surface coordination of certain surfactant molecules used in the growth of the nanocrystals.[62−72] For example, the groups of Hens, Owen, and Weiss have used NMR spectroscopy to identify the binding modes of various alkyl ligands containing amine, carboxylic, and/or phosphonic acid on hydrophobic CdSe nanocrystals.[68,70,73−76] Additional solution phase NMR spectroscopy measurements were used to control or monitor ligand exchange and the stability of nanocrystals in polar solvents. Reiss and co-workers probed the effects of deprotonating the thiol groups in the capping ligand, via pH adjustment, on the strength of binding of cysteine molecules to QD surfaces and showed that this affects their colloidal stability in water media.[77] Similarly, Van Driessche, De Roo, and co-workers investigated the use of small amino acids as ligands to promote a ligand exchange-driven phase transfer of carboxylic acid-capped HfO_2 and ZrO_2 nanocrystals to various polar solvents.[78]

Here, we detail the combined use of ^{1}H NMR, diffusion ordered spectroscopy (DOSY), two-dimensional ^{13}C−^{1}H heteronuclear single-quantum coherence (HSQC), and ^{31}P NMR spectroscopy techniques to characterize the structure and density of several hydrophilic CdSe-ZnS core−shell QDs that have been ligand exchanged with lipoic acid appended with polyethylene glycol (LA-PEG) ligands. More precisely, three sets of polyethylene glycol-modified lipoic acid ligands with distinct architectures have been tested: LA-PEG-OCH_3, bis(LA)-PEG-OCH_3, and LA-(PEG-OCH_3)$_2$. DOSY and HSQC measurements were first applied to distinguish between bound and free molecules in the medium, to identify the most informative protons in the ligands, and to account for potential signature overlap between distinct protons upon ligand binding. We further exploited the sharp ^{1}H signature(s) of the laterally extended terminal groups compared to various external standards, to estimate the number of ligands per nanocrystal. Three sets of core−shell QDs photoligated with these ligands have been characterized. We have investigated the effects of the QD surface curvature and structure of the ligand on the overall footprint area per ligand and found that all these parameters affect the ligand arrangements in these systems.

EXPERIMENTAL SECTION

Materials. Tri-*n*-octylphosphine oxide (TOPO, 99%), tri-*n*-octylphosphine (TOP, 90% and 97%), *n*-hexylphosphonic acid (HPA), cadmium acetylacetonate [Cd(acac)$_2$, 98%], selenium metal (99.99%), hexamethyldisilathiane [(TMS)$_2$S, 98%], sodium azide, and 1-hydroxybenzotriazole monohydrate (HOBt·H_2O) were purchased from Alfa Aesar (Ward Hill, MA). Tri-*n*-octylphosphine oxide (TOPO, 90%) and diethylzinc (99.9998%) were purchased from Stream Chemical Inc. (Newburyport, MA). 1-Hexadecylamine (HDA, 90%) and 1,2-hexadecanediol (HDDO, 90%) were purchased from Sigma Chemicals (St. Louis, MO). Poly(ethylene glycol)methyl ether (average molecular weight of ∼750 Da), L-aspartic acid, (±)-α-lipoic acid, *N*,*N*-dicyclohexylcarbodiimide (DCC), 4-(*N*,*N*-dimethylamino)-pyridine (DMAP), di-*tert*-butyl dicarbonate (Boc_2O), trifluoroacetic acid (99%), triphenylphosphine (TPP), ethylenediamine, 4 M HCl in dioxane, triethylamine, tetramethylammonium hydroxide (TMAH), sodium benzoate (>99%), NaCl, $KHSO_4$, $KHCO_3$, anhydrous Na_2SO_4, and organic solvents (chloroform, methanol, ethanol, hexane, tetrahydrofuran, ethyl acetate, dioxane, *N*,*N*-dimethylformamide, diethyl ether, etc.) were also purchased from Sigma Chemicals. Column purification chromatography was performed using silica gel (60 Å, 230−400 mesh, Bodman Industries, Aston, PA). (Trimethylsilyl)propionic-2,2,3,3-d_4 acid sodium salt (TMSP-d_4, 99%) and deuterated solvents (e.g., chloroform-*d* and D_2O) used for NMR experiments were purchased from Cambridge Isotope Laboratories Inc. (Andover, MA). Ultrapure water used for all experiments was obtained from a Milli-Q Integral 5 system. Moisture- and air-sensitive materials were handled in an MBraun (Stratham, NH) Labmaster 130 glovebox. Air-sensitive reactions were performed using standard Schlenk techniques.

Growth of CdSe-ZnS Core−Shell Quantum Dots. The CdSe-ZnS core−shell QDs were prepared in two steps using the hot injection method, as described in previous literature protocols.[22,79−82] First, the organometallic precursors consisting of cadmium acetylacetonate [Cd(acac)$_2$] and trioctylphosphine-selenium (TOP:Se) were reduced at a high temperature (∼350 °C) in a coordinating solvent mixture, consisting of TOP, TOPO, HDA, and HDDO, to grow the CdSe cores. The cores were then overcoated with a few monolayers of a ZnS shell (approximately five or six monolayers) using Et_2Zn and TMS_2S precursors at lower temperatures (150−180 °C). Further description of the growth reaction is provided in the Supporting Information.

Synthesis of the PEG-Modified LA Ligands. Three sets of PEG-modified LA ligands, containing one or two lipoic acid (LA) anchors and one or two polyethylene glycol moieties, were prepared and tested in this study.[41,45] All compounds were purified using silica gel chromatography.[41,45,46,83] LA-PEG_{750}-OCH_3 (**L1**) was synthesized starting from commercially available methoxy-PEG_{750}-OH following the protocol reported in ref 45. Briefly, the terminal hydroxyl group of methoxy-PEG_{750}-OH was first converted to azide and then transformed to amine. This amine was further attached to lipoic acid via *N*,*N*-dicyclohexylcarbodiimide (DCC) coupling to provide LA-PEG-OCH_3. LA-(PEG-OCH_3)$_2$ (**L2**) was prepared starting from L-aspartic acid as a precursor, following the method introduced in our previous report.[41] Briefly, the amine moiety in the L-aspartic acid was coupled to

DOI: 10.1021/acs.chemmater.8b01033
Chem. Mater. 2018, 30, 3454−3466

Boc_2O (i.e., BOC protection) to reduce the effects of cross-coupling reactions. Then, 2 equiv of NH_2-PEG-OCH_3 was added to install two PEG chains onto the Boc-aspartic acid, via DCC coupling. Subsequently, deprotection of the amine group was performed using 4 M HCl in dioxane, followed by coupling to 1 equiv of lipoic acid, yielding the compound LA-(PEG-OCH_3)$_2$. Bis(LA)-PEG-OCH_3 (**L3**) was also synthesized using the same L-aspartic acid precursor, but following a slightly modified protocol.[41] In the first step, 1 equiv of NH_2-PEG-OCH_3 was mixed with BOC-protected aspartic acid to modify one carboxyl group with a PEG block. The second carboxyl was coupled to LA-ethylenediamine. After BOC deprotection using dioxane/HCl, a second lipoic acid was attached to the amine group via DCC coupling, yielding bis(LA)-PEG-OCH_3.

Photoligation of QDs with PEGylated LA Ligands and NMR Sample Preparation. In situ photochemical transformation of lipoic acid combined with ligand exchange was used to substitute the hydrophobic coating and transfer the QDs to aqueous media. This photoinduced strategy exploits the sensitive nature of the LA moieties under ultraviolet (UV) irradiation, where photochemical transformation of the dithiolane groups alters the disulfide bond and facilitates ligation on the QD surfaces.[84] Additional details are provided in the Supporting Information.

To prepare the samples for NMR experiments, the QDs were dried and transferred to deuterated solvents; e.g., DI (deionized) water was replaced with D_2O. For the latter, three rounds of concentration and dilution with D_2O using a centrifugal membrane filtration device (molecular weight cutoff of 50 kDa, Amicon Ultra, Millipore) were applied; this removes H_2O and excess free solubilized ligands from the sample. The resulting dispersions were then transferred to a 5 mm diameter 600 MHz NMR tube and used to collect the spectra. The same protocol was used to prepare hydrophilic QDs capped with LA-PEG-OCH_3, LA-(PEG-OCH_3)$_2$, or bis(LA)-PEG-OCH_3.

Analytical Measurements. The ultraviolet−visible (UV−vis) absorption spectra were recorded using a Shimadzu UV−vis absorption spectrophotometer (UV 2450 model, Columbia, MD). A Fluorolog-3 spectrometer (Jobin Yvon Inc., Edison, NJ) was used to measure the fluorescence spectra. The photoligation experiments were conducted in a UV photoreactor (emission band centered at 350 nm, 4.5 mW/cm^2, model LZC-4 V, Luzchem Research Inc., Ottawa, ON). A lab-scale rotary evaporator (R-215, Buchi, New Castle, DE) was used to concentrate or dry the various ligand solutions and QD dispersions.

NMR Spectroscopy Measurements. All NMR spectra were recorded using a Bruker Avance III HD 600 MHz spectrometer equipped with a 5 mm z-gradient Broad Band Observe (BBO) probe (Bruker SpectroSpin, Billerica, MA) operating at 600.13 MHz (for the ^{1}H frequency) and 242.9 MHz (for the ^{31}P frequency). All spectroscopic measurements were taken at room temperature (∼293.5 K). The ^{1}H NMR spectra were recorded using a 90° high-power pulse with a duration of 13.0 μs, an acquisition time of 1.5 s, and a delay time d_1 of 6 s. A line broadening of ∼0.3 Hz (i.e., <1 Hz) was applied before the Fourier transform was performed. The delay time mentioned above was determined using the requirement $d_1 > 5T_1$ (T_1 is the spin−lattice relaxation time), to ensure that sufficiently long recovery delays are met. The T_1 measurements were optimized using the pulse program "t1ir1d".

The two-dimensional (2D) ^{13}C−^{1}H heteronuclear single-quantum coherence (HSQC) spectra were recorded using a standard Bruker pulse sequence "hsqcetgpsi.2" with a 10 s 90° pulse width, a 2 s pulse delay, and a 145 Hz $^1J_{C-H}$. The HSQC data were acquired with 2048 data points (for ^{1}H) and 256 increments (for ^{13}C). The solvent (H_2O) residue peak was used for chemical shift calibration. The diffusion ordered spectroscopy (DOSY) data were collected at room temperature (293.5 K) using gradient pulse sequences "stebpgp1s" with a 5 s relaxation delay and four dummy scans. The 90° pulse width was calibrated for each DOSY experiment typically over the range of 10−13 s. Each 2D slice represents the signal average over 16 scans. The gradient duration and diffusion time vary for different samples. The diffusion time depends on the T_2 relaxation times of the resonances in the spectrum (∼100−300 ms). Typical experimental parameters used for data from yellow-emitting CdSe-ZnS QDs were as follows: gradient strength of 45 G/cm, diffusion time of 200 ms, and gradient pulse length of 3 ms. The number of steps for the ramp is between 32 and 64. Manual baseline corrections were made to minimize the experimental error. The residual H_2O peak was used as an internal diffusion coefficient reference. Similar experimental parameters were applied for all QD samples.

RESULTS AND DISCUSSION

Rationale and Motivation. Postsynthetic surface modification of colloidal nanocrystals (e.g., luminescent QDs and plasmonic nanocrystals) with a hydrophilic coating is an integral part of interfacing them with biology. Phase transfer promoted by ligand exchange of the native capping surfactants with hydrophilic ligands, which is primarily driven by competitive coordination interactions, is highly effective. This strategy promotes steric stabilization of the nanocrystals (as nanocolloids), while endowing them with biocompatibility. The nature and spatial arrangement of the surface ligands affect the long-term colloidal stability, determine their hydrodynamic size, and impart surface functionality onto such nanomaterials. Furthermore, because there is a dynamic on−off equilibrium between surface-bound and freely diffusing ligands in the dispersion, the arrangement of the ligands on the nanocrystal surfaces can be affected by the molecule size and architecture, the coordination affinity, and the surrounding environment.

Characterization of the ligand coating of various nanomaterials has focused on determining the ligand density, but often "disruptive" techniques have been employed to achieve this aim. For example, in an earlier study, we combined dye labeling with UV−vis absorption to extract a measure of the density of LA-PEG ligands on AuNPs. Citrate-capped nanoparticles were exchanged with a mixture of LA-PEG-methoxy and LA-PEG-maleimide ligands followed by coupling of the ligand to a cysteine peptide dye.[85] In another study, we applied a slightly different strategy to quantify the density of LA-PEG ligands on luminescent QDs.[86] We relied on hydrazone ligation between aldehyde-modified LA-PEG on the QDs with 2-hydrozinopyridine, which promoted the formation of bound hydrazone chromophores with a defined absorption at 350 nm. Other studies used a variety of approaches, including dye labeling via EDC coupling between amines and NHS ester dyes.[70] These techniques encounter a few natural hurdles, in particular when using methods that rely on dye labeling, as this introduces additional steric constraints and may yield underestimated ligand density values. Therefore, a nondisruptive and easy to implement analytical tool is required to provide a true characterization of the organic coating layer.

NMR is nondisruptive, as it does not introduce additional labels, and its use to characterize molecules and colloidal nanomaterials in solution has attracted intense interest.[70,71,74,87,88] With the recent advances in NMR instrumentation and the increased sensitivity of the technique, solution phase NMR spectroscopy can non-invasively probe the surface coating under various conditions. Our study aims to address a few questions. (1) What degrees of post-phase transfer purification are required to yield samples in which only bound ligands are accounted for in the NMR measurements while sterically stabilized nanoparticle dispersions are maintained? (2) How does the coordination number and steric hindrance of the hydrophilic block in the ligand structure affect the surface coverage? (3) Does the surface curvature of the QD play a role in determining the footprint area of the surface-

DOI: 10.1021/acs.chemmater.8b01033
Chem. Mater. 2018, 30, 3454−3466

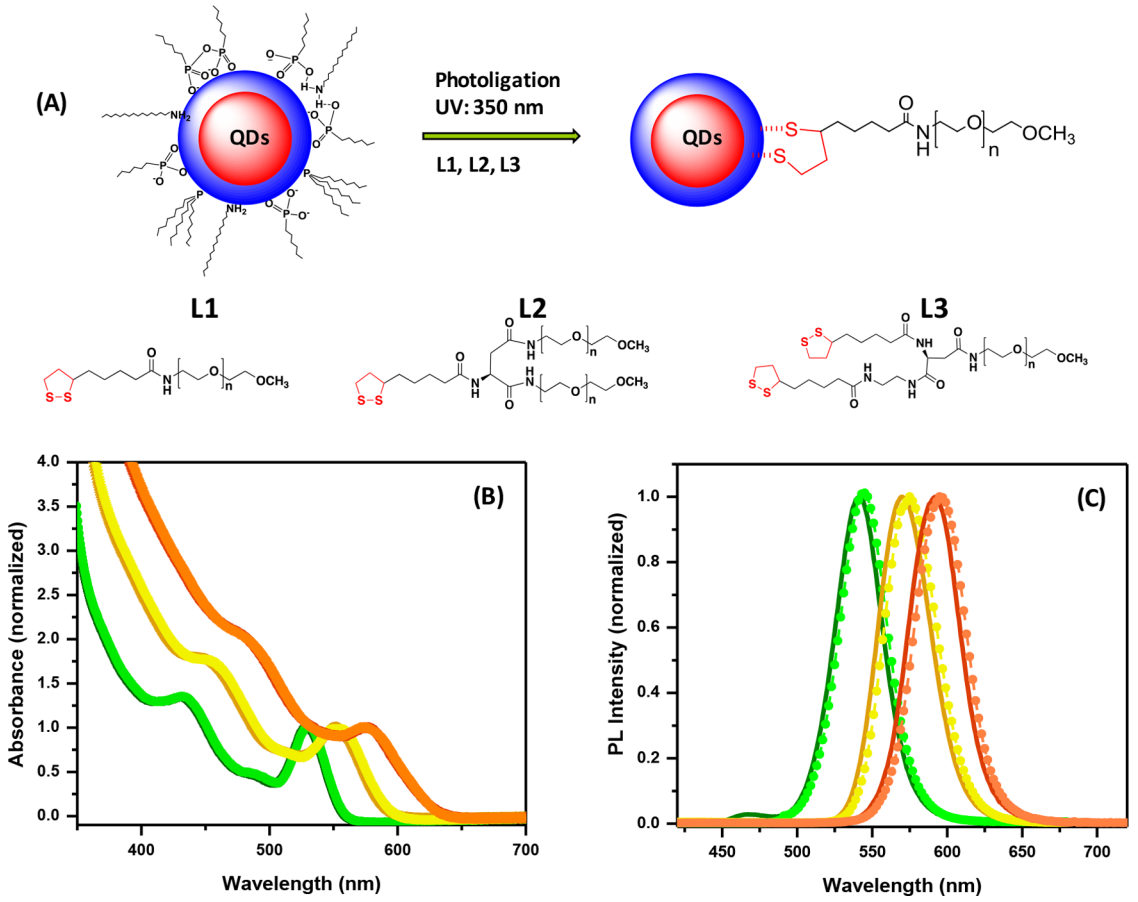

Figure 1. (A) Schematic representation of the phase transfer route from organic to buffer media, promoted by photoinduced ligand exchange. Chemical structures of three sets of lipoic acid-based ligands used, namely, LA-PEG-OCH_3 (**L1**), LA-$(PEG\text{-}OCH_3)_2$ (**L2**), and bis(LA)-PEG-OCH_3 (**L3**). (B) Absorption and (C) emission spectra of green-emitting (λ_{em} = 536 nm), yellow-emitting (λ_{em} = 570 nm), and orange-emitting (λ_{em} = 590 nm) QDs. The absorption and emission spectra are normalized with respect to the values at the band edge absorption and PL peaks, respectively. The solid lines represent the native hydrophobic QDs in toluene. The dotted lines with symbols are spectra collected from hydrophilic QDs photoligated with LA-PEG-OCH_3.

bound ligands? For this, we applied a few NMR spectroscopy techniques to characterize three sets of QDs with distinct emission, surface coated with three PEG-modified LA-based ligands with variation in the coordination number and size of the hydrophilic block (see Figure 1).

Optical Characterization of the QDs. We used three sets of core−shell QDs with PL emission centered at 536 nm (green QDs), 570 nm (yellow QDs), and 590 nm (orange QDs). The phase transfer relied on photoligation of the hydrophobic nanocrystals with three sets of polyethylene glycol-modified lipoic acid ligands: LA-PEG-OCH_3 (one anchor and one PEG block, **L1**), LA-$(PEG\text{-}OCH_3)_2$ (one anchor and two PEG chains, **L2**), and bis(LA)-PEG-OCH_3 (two anchors and one PEG block, **L3**) (see Figure 1). Ligand exchange was promoted by photochemical transformation (reduction) of the lipoic acid groups under UV irradiation (using a band centered at 350 nm) and in situ substitution of the native hydrophobic cap with the PEGylated ligands. Following ligand exchange, the hydrophilic QDs were purified from free ligands and remnant solubilized hydrophobic cap by applying up to three rounds of dilution and concertation with deionized water or D_2O, using a membrane filtration device (Millipore, Amicon Ultra, molecular weight cutoff of 50 kDa).[84] The QDs were then characterized using UV absorption and fluorescence spectroscopy measurements. Panels B and C of Figure 1 show the absorption and PL spectra of the three sets of QDs dispersed in toluene and in water, respectively, after ligand exchange. Spectra indicate that the main absorption characteristics of the QDs, namely, the location and shape of the excitonic peaks, are preserved. Similarly, the emission profiles collected from the hydrophilic nanocrystals are essentially identical to those measured from hydrophobic QDs. Overall, these results confirm that the photoligation strategy does not alter the structure or the photophysical properties of the nanocrystals.

Characterization of the QD Coating Using NMR Spectroscopy. We applied four complementary solution phase NMR techniques to carefully characterize the hydrophilic coating on the nanocrystals, namely, ^{1}H NMR, ^{31}P NMR, DOSY NMR, and HSQC spectroscopies. This combination is paramount for proving that only surface-bound ligands are characterized in the medium, for verifying that all phosphorus-containing organic surfactants are removed during ligand exchange, and for extracting quantitative estimates for the ligand density per nanocrystal. It also allows a direct comparison between the signatures of the ligands when they are surface-ligated or freely diffusing in the dispersion.

Combined Solution Phase One-Dimensional and DOSY NMR Spectroscopy. Solution phase ^{1}H 1D and DOSY NMR measurements were used to identify the optimal sample

DOI: 10.1021/acs.chemmater.8b01033
Chem. Mater. 2018, 30, 3454−3466

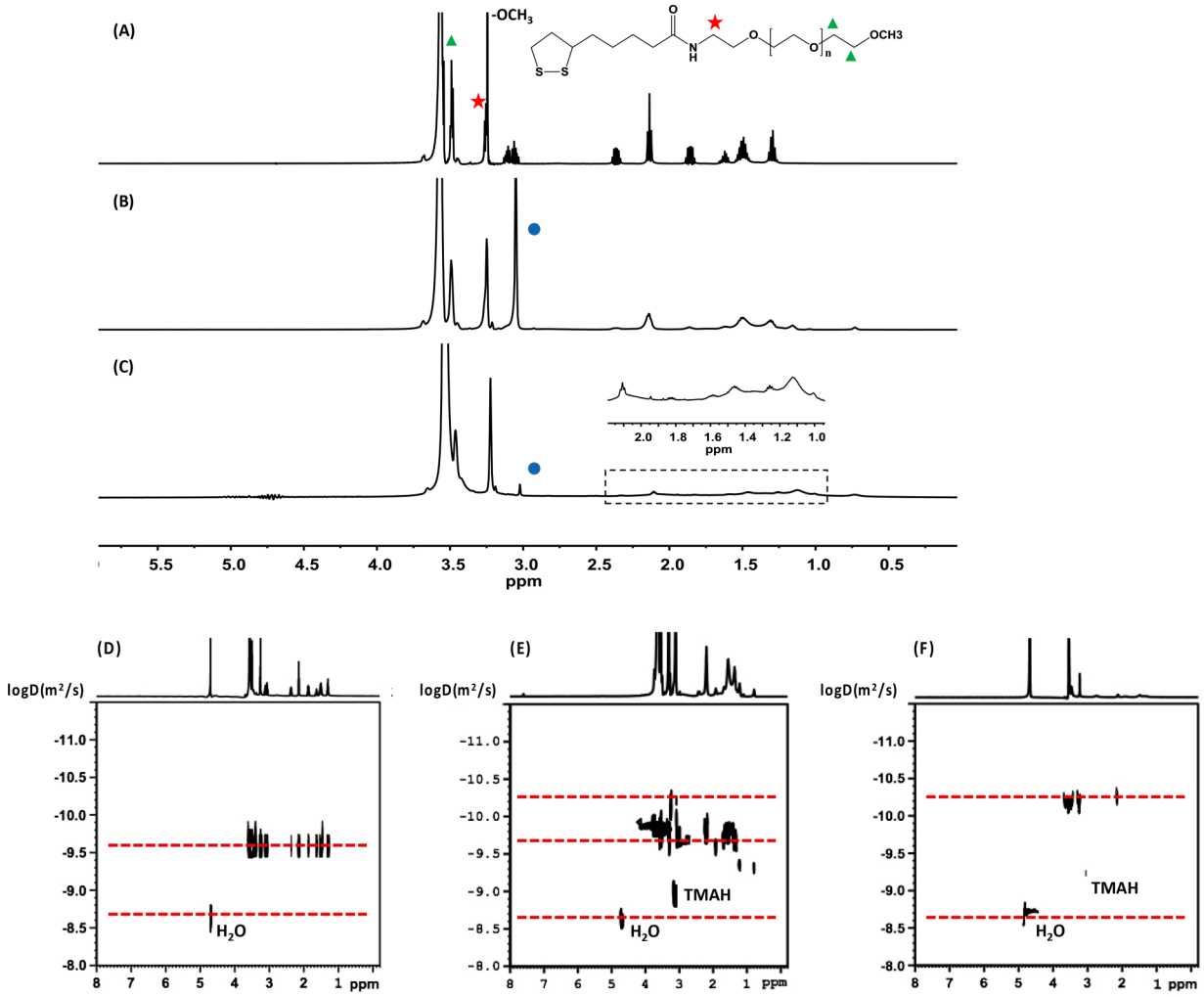

Figure 2. ^{1}H NMR spectra of LA-PEG-OCH_3 solution (A) together with LA-PEG-OCH_3 QD dispersions in D_2O, after one round (B) and two rounds (C) of purification. DOSY spectra of LA-PEG-OCH_3 in D_2O (D), side by side with LA-PEG-OCH_3 QD dispersions also in D_2O after one round (E) and two rounds of purification (F). Note that the signal in panel E is dominated by the contribution from free ligands. Yellow-emitting QDs were used. The blue circle designates impurities. The NMR spectra recorded in D_2O are water-suppressed.

conditions under which only surface-coordinated ligands are probed and characterized. For this, we start by comparing the ^{1}H NMR spectra collected from a solution of free LA-PEG-OCH_3 in D_2O with those collected from dispersions of QDs (green-, yellow-, or orange-emitting) photoligated with the same ligand and subjected to zero to three rounds of purification using membrane filtration (see the Experimental Section for more details). The 1D spectra are supplemented with DOSY NMR measurements applied to solutions of free ligands, or to the QD dispersions. The ^{1}H NMR spectra in Figure 2A–C show that the main proton signatures ascribed to the PEG block and the terminal methoxy group are measured for both free and surface-bound ligands, though with slight shifts: the proton PEG peak is at ∼3.6 ppm for free ligands but shifts to ∼3.55 ppm when the ligands are surface-bound. Similarly, the OCH_3 peak measured for free ligands at 3.3 ppm is shifted to 3.2 ppm when the ligands are bound. There is also a sizable broadening combined with weakening of all measured signatures for the data collected from the purified QD dispersions, in particular in the range of 1–3 ppm, where the peaks of the lipoic acid protons are found. This implies that broadening and weakening of the NMR features drastically affect the signatures emanating from protons in the bound ligand that are closer to the nanocrystal surfaces. In addition, those spectra show the absence of any peaks in the range of 0–1 ppm, which suggests that the native hydrophobic ligands (e.g., TOPO, TOP, HPA, and HDA) have essentially been removed from the medium.[89,90] Removal of the native ligands from the samples was further supported by ^{31}P NMR spectra collected from the purified QD dispersions, where no signatures of the phosphorus-containing compounds were detected (see Figure S1).[90]

Although broadening of resonance peaks is a general feature of ligands (i.e., protons) associated with larger objects (here, the nanocrystals), this property alone does not provide unequivocal evidence that those ligands are indeed surface-bound. Phase transfer driven by ligand exchange uses a large excess of ligands compared to the QDs, and contributions from free ligands (present in the medium) to the NMR spectra can interfere with data analysis and characterization of the coating. Reliable purification techniques must be applied to discard those free ligands without affecting the colloidal integrity or photophysical properties of the dispersions. Thus, prior to discussing the arrangement and stoichiometry of the ligand shell, we exploit the ability of DOSY NMR to differentiate between free and surface-coordinated ligands in a solution

DOI: 10.1021/acs.chemmater.8b01033
Chem. Mater. 2018, 30, 3454–3466

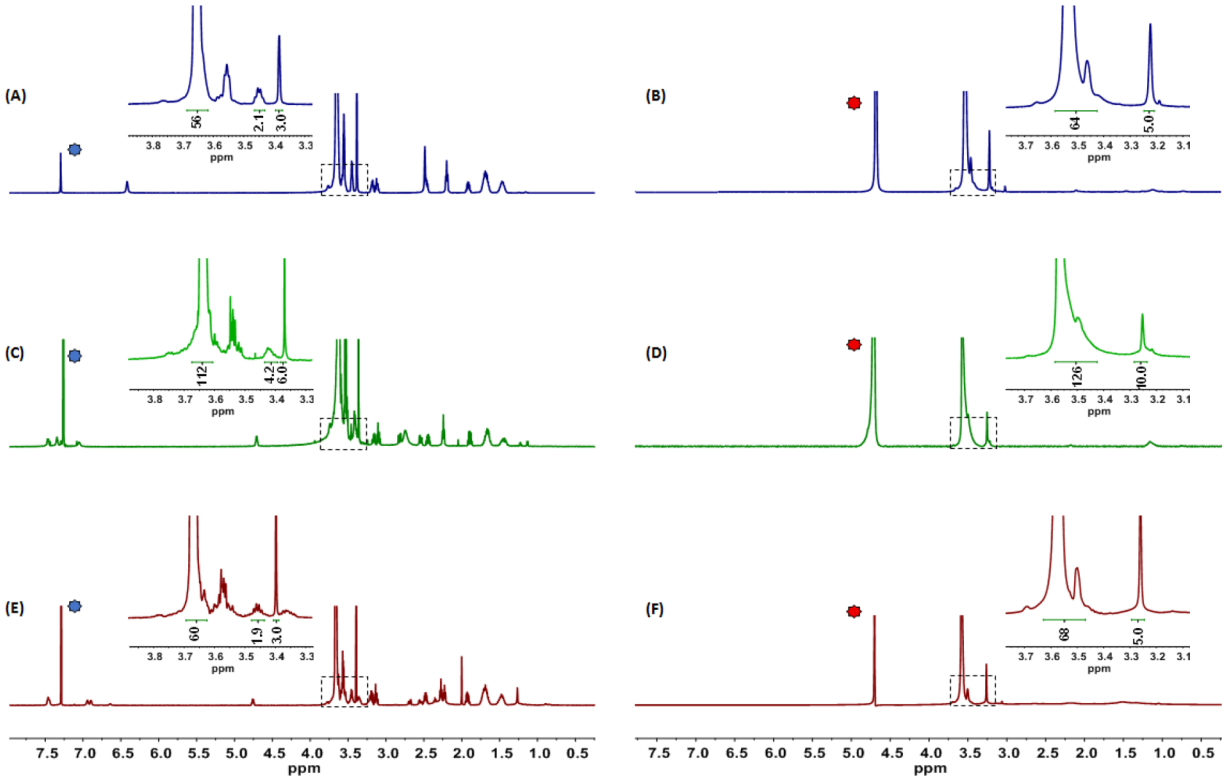

Figure 3. ^{1}H NMR spectra of (A) LA-PEG-OCH_3, (C) LA-$(PEG\text{-}OCH_3)_2$, and (E) bis(LA)-PEG-OCH_3 in chloroform-*d* solutions, along with spectra of (B) LAPEG-OCH_3 QDs, (D) LA-$(PEG\text{-}OCH_3)_2$ QDs, and (F) bis(LA)-PEG-OCH_3 QDs dispersed in D_2O. All three QD dispersions were subjected to three rounds of purification prior to collection of the spectra. Yellow-emitting QDs have been used for these measurements. The labels in the left and right panels designate the solvent peak ($CHCl_3$ for the pure ligand and H_2O for the dispersions). Also apparent in the ligand spectra (~4.75 ppm, C and E) is the signature of the α proton in the aspartic acid. The boxes outline the ppm range included in the expanded windows, not the intensities.

sample based on Brownian diffusion and outline the conditions under which the identified ligands in purified samples emanate primarily from surface-bound molecules. The diffusion coefficients of free ligands and ligands bound to a nanocrystal can be obtained from diffusion-ordered NMR spectroscopy (DOSY), as described in refs 91 and 92. Figure 2D shows the DOSY spectrum of LA-PEG-OCH_3 (**L1**) dissolved in D_2O (without QDs), represented as a contour plot of the signal intensity correlating the proton chemical shift with the corresponding diffusion coefficient. All the proton signals of LA-PEG-OCH_3 are associated with the same diffusion coefficient. Panels E and F of Figure 2 show the DOSY spectra of a dispersion of LA-PEG-OCH_3-capped QDs (yellow-emitting) subjected to one and two rounds of purification. In the QD sample subjected to two rounds of purification, we observe only one diffusion coefficient for all the detected protons that is approximately 1 order of magnitude slower than the value extracted for free LA-PEG-OCH_3 (compare panels D and F in Figure 2). Similar data were collected from QDs photoligated with **L2** and **L3** and then subjected to three rounds of purification (see Figure S2). This can be attributed to the slower Brownian motion of the QD−ligand complex. Furthermore, the absence of a signature associated with a faster diffusion coefficient proves that there is no detectable free ligand in the water dispersion of QDs after two or more rounds of purification. In comparison, the DOSY spectrum collected from a dispersion of QDs subjected to zero or one round of purification shows two distinct diffusion coefficients, one associated with the free ligand and the other with the QD-bound ligand (as shown in Figure 2E). These results combined with the pronounced peak broadening indicate that no detectable free cap is measured in samples subjected to at least two rounds of purification. These findings prove the effectiveness of the photoligation strategy in substituting the native cap with the hydrophilic ligands and imply that tight ligand coordination on the ZnS-rich surface drives the binding. Characterization of the ligand stoichiometry on the QD surfaces will be applied to samples that have been subjected to two or three rounds of purification.

Panels A, C, E and B, D, F of Figure 3 show the 1D ^{1}H NMR spectra collected from LA-PEG-OCH_3, LA-$(PEG\text{-}OCH_3)_2$, and bis(LA)-PEG-OCH_3 ligands, respectively, in $CDCl_3$ solutions (which serve as references) side by side with representative NMR spectra collected from purified aqueous dispersions of QDs (yellow-emitting) capped with those ligands. Additional ^{1}H NMR spectra collected from dispersions of green- and orange-emitting QDs are provided in Figure S4. The signatures present in the upfield region (1−3 ppm) measured for all three ligands correspond to the lipoic acid protons, whereas the peaks in the range of ~3.3−3.8 ppm are assigned to the protons in the terminal methoxy and the PEG methylene groups, as shown above. Furthermore, a few of the proton resonances in the spectra of the QD dispersions, shown in panels B, D and F, are shifted upfield and substantially broadened compared to the signature observed in the spectra of free ligands. For surface-bound ligands, interproton dipolar interactions near the nanocrystal surface are strongly enhanced because of the reduced rotational mobility, which results in faster transverse

DOI: 10.1021/acs.chemmater.8b01033
Chem. Mater. 2018, 30, 3454−3466

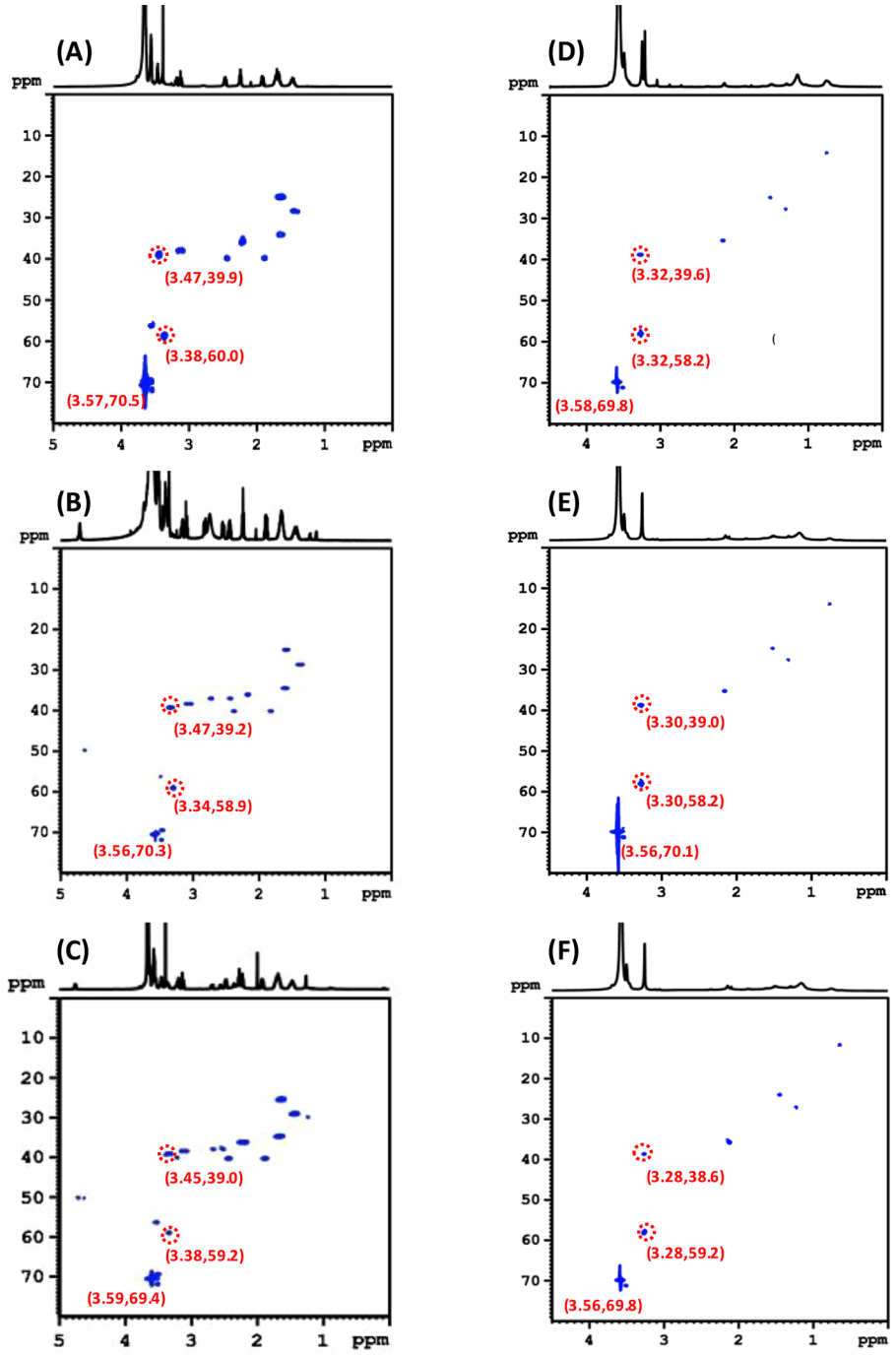

Figure 4. HSQC spectra collected from ligand solutions in chloroform-*d* of (A) LA-PEG-OCH_3, (B) LA-$(PEG\text{-}OCH_3)_2$, and (C) bis(LA)-PEG-OCH_3 and HSQC spectra of (D) LA-PEG-OCH_3 QDs, (E) LA-$(PEG\text{-}OCH_3)_2$ QDs, and (F) bis(LA)-PEG-OCH_3 QDs dispersed in D_2O. Yellow-emitting QD dispersions subjected to three rounds of purification have been used. Note that the signatures measured for the QD-bound ligands are weaker as expected because of slower dynamics. We should also note that for spectra collected from **L2** (B) and **L3** (C) in $CDCl_3$ there is a signature at ~4.75 ppm (^1H) and ~50 ppm (^{13}C) ascribed to the α proton of the aspartic acid moiety in the ligands.

relaxation and produces peak broadening and weakening of the signal.[93] The resonances ascribed to the lipoic acid moiety, in the range of 1−3 ppm, show weak peak intensities combined with pronounced line broadening, making identification of those signatures rather difficult. Conversely, because of their location at the end of a flexible PEG bridge (thus farther from the surface), the terminal methoxy protons experience faster dynamic motions compared to those closer to the nanocrystal surface. They yield a sharp peak at ~3.30 ppm. However, line broadening combined with the upfield shift of proton signatures in the ligands, due to the presence of a different chemical environment surrounding the nanocrystal surface, may create a significant overlap between the peaks associated with the methoxy protons and those in their proximity [namely, methylene unit around the PEG block (see Figure 2A)]. For instance, examination of the spectra shown in Figures 2 and 3 indicates that there is more overlap between the signatures of the PEG protons at ~3.65 ppm, and the adjacent methylene peak at ~3.55 ppm, as well as merger and/or overlap between the -O$\underline{CH_3}$ and the -CONH-$\underline{CH_2}$ protons for surface-

DOI: 10.1021/acs.chemmater.8b01033
Chem. Mater. 2018, 30, 3454−3466

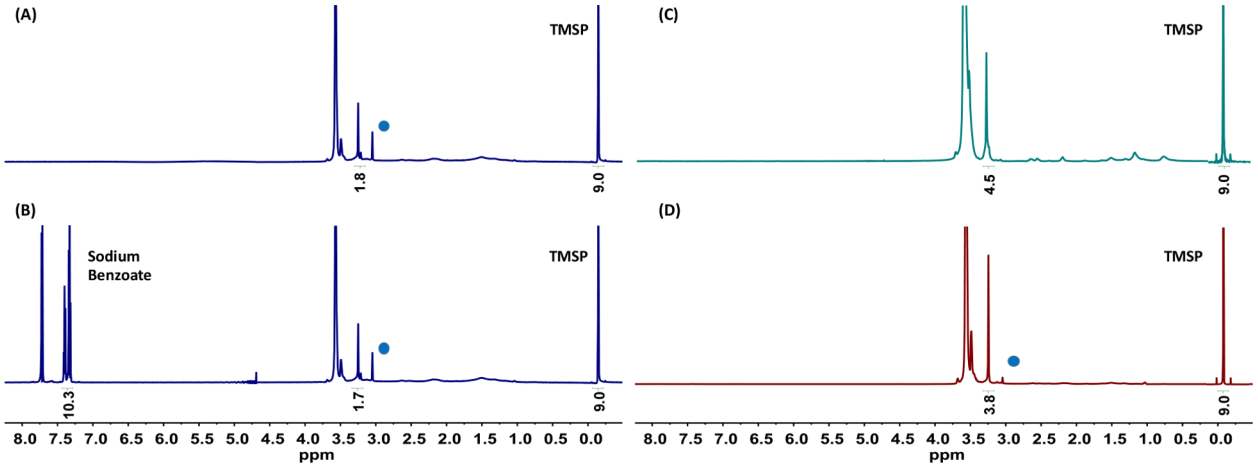

Figure 5. Estimates of the number of ligands per nanocrystal are extracted by comparing the peak integration for the QD dispersions to those of a standard. Shown are ^{1}H NMR spectra of (A) LA-PEG-OCH_3 QDs mixed with TMSP, (B) LA-PEG-OCH_3 QDs mixed with TMSP and sodium benzoate, (C) LA-$(PEG\text{-}OCH_3)_2$ QDs mixed with TMSP, and (D) bis(LA)-PEG-OCH_3 QDs mixed with TMSP. The nanocrystals were subjected to three rounds of purification and dispersed in D_2O followed by addition of the standard(s). The blue circle designates impurities. Yellow-emitting QDs were used to collect the data.

coordinated ligands. Such overlap will alter the total proton integration for those peaks in D_2O and affect the estimates for the ligand density extracted from the NMR data. To address this issue and gain a better understanding of the peak assignments for bound ligands, we resort to additional 2D NMR measurements.

Remark: We collected the ^{1}H NMR spectra of the pure ligands in $CDCl_3$ solutions, because bis(LA)-PEG, the oxidized form of this compound, has limited solubility in water. The QDs photoligated with all three ligands are completely dispersible in aqueous media.

Heteronuclear Single-Quantum Coherence (HSQC) Spectroscopy. This technique probes the correlation between the ^{1}H and ^{13}C signatures in the NMR spectra, thus allowing one to distinguish between protons that belong to two distinct methylene groups in the same LA-PEG molecule. This approach exploits the fact that the ^{13}C signatures are well-separated due to the wider window of chemical shifts on the ^{13}C scale.[94] Panels A and D of Figure 4 show the HSQC spectra of free LA-PEG-OCH_3 side by side with QDs photoligated with the same ligand and dispersed in D_2O. The ^{13}C chemical shifts of all characteristic peaks for the ligand are overall comparable to those measured from the QD dispersion. However, we found that for the QD sample the two distinct ^{13}C resonances at 60 and 40 ppm ascribed to -O$\underline{C}H_3$ and the methylene group in -CONH-$\underline{C}H_2$ correspond to closely located proton peaks (i.e., at ∼3.32 ppm). In contrast, the spectrum of the free ligands shows that the ^{1}H signatures for those two groups have no overlap (i.e., O$\underline{C}H_3$ at ∼3.38 ppm and NH-$\underline{C}H_2$ at ∼3.47 ppm). The HSQC spectra for the other two sets of QD ligands [using LA-$(PEG\text{-}OCH_3)_2$ or bis(LA)-PEG-OCH_3] show similar behaviors, with peak broadening and a slight upfield shift of the proton signatures, combined with ^{13}C overlap between the signatures of the methoxy and methylene protons [i.e., overlap of the O$\underline{C}H_3$ and NH-$\underline{C}H_2$ protons at ∼3.28−3.30 ppm (see panels C and D and panels E and F of Figure 3)].

These findings can further be complemented with analysis of the peak integration ratios of the terminal group and PEG block. For example, the measured integration ratio of the proton peaks of the PEG chain (at ∼3.6−3.7 ppm) and terminal methoxy (at ∼3.38 ppm) for the free ligand is 56:3. In comparison, the ratio measured for the protons ascribed to the QD-bound ligands (the combined PEG and methylene proton peak at ∼3.45−3.65 ppm and methoxy and methylene peak at ∼3.28−3.30 ppm) is ∼64:5; note that the integration peak of the PEG moiety (mPEG, molecular weight of 750) should be ∼58−65, accounting for the inherent polydispersity of these chains. This indicates that there is clear overlap between two proton peaks when the ligands are coordinated on the nanocrystal surfaces and dispersed in D_2O. Similarly, the integration values for QDs photoligated with LA-$(PEG\text{-}OCH_3)_2$ or bis(LA)-PEG-OCH_3 were calculated from the spectra in panels B and E and panels C and F of Figure 3, respectively. For both sets of QD dispersions, the integration ratio of the PEG protons located at 3.4−3.7 ppm and methyl and methylene peaks located 3.2−3.3 ppm is ∼126:10 for ligand **L2** and 68:5 for ligand **L3** (see Figure 3). In addition to the broad resonances, a low signal-to-noise ratio of the peaks in the range of ∼1−3 ppm was observed. Overall, these subtle changes are rather important for collecting accurate data on the density of surface ligands extracted from the various ^{1}H NMR spectra.

Quantification of Ligand Packing on the Nanocrystals. Having proven that the NMR signatures ascribed to the methoxy-PEG chains, measured for purified QD dispersions, emanate from only QD-bound ligands and identified which protons in the ligands are most affected by surface coordination, we now proceed to extract estimates for the ligand density using our present set of data. For this, we compare the integrated peak intensity associated with the combined methoxy and methylene proton signatures at ∼3.2−3.3 ppm (see Figure 5) to the peak intensity measured for a standard compound (added externally) at a known concentration. Here, we discuss the ligand quantification data in comparison to TMSP as a standard, because its signature is far from those of the methoxy and methylene protons of the ligands. Nonetheless, comparison to another standard, sodium benzoate, was also performed to provide better confidence in the data analysis and extracted information (see Table S1 and Figure S5).

The procedure described above provides a measure for the overall concentration of QD-coordinated ligands, which is then

DOI: 10.1021/acs.chemmater.8b01033
Chem. Mater. 2018, 30, 3454−3466

compared to the molar concentration of the QDs,[86,95] yielding a value for the average number of ligands per nanocrystal. The QD concentration is extracted from the UV absorption spectra of each set of QDs and using the corresponding molar extinction coefficients at 350 nm:[95] ε_{350} (green QDs) = 7.53 × 10^5 M^{-1} cm^{-1}, ε_{350} (yellow QDs) = 9.42 × 10^5 M^{-1} cm^{-1}, and ε_{350} (orange QDs) = 15.7 × 10^5 M^{-1} cm^{-1}. The sizes of the core−shell QDs were extracted from a combination of X-ray scattering at small angles and the overcoating shell thickness.[22,96] The numbers of bound ligands per nanocrystal extracted for the nine sets of QD−ligand pairs using the NMR data analysis described above are listed in Table 1.

Table 1. Estimates of the Numbers of Ligands per QD Along with the Corresponding Ligand Densities and Footprint Areas (FPAs) per Capping Molecule Associated with Each QD−Ligand Set, Extracted from the Various NMR Analyses[a]

QD set	ligand	ligand number	ligand density (nm^{-2})[b]	FPA (nm^2)[c]
green QDs (λ_{em} = 536 nm) (radius ≅ 3 nm)	**L1**	154 ± 20	1.36	0.73
	L2	71 ± 12	0.63	1.59
	L3	88 ± 13	0.78	1.28
yellow QDs (λ_{em} = 570 nm) (radius ≅ 3.4 nm)	**L1**	281 ± 31	1.93	0.52
	L2	157 ± 9	1.08	0.92
	L3	174 ± 22	1.19	0.83
orange QDs (λ_{em} = 590 nm) (radius ≅ 3.6 nm)	**L1**	370 ± 37	2.27	0.44
	L2	235 ± 21	1.44	0.69
	L3	280 ± 23	1.72	0.58

[a]TMSP was used as a standard for these measurements and analyses. The values for the QD core-shell radius were extracted from previous small angle X-ray scattering data and assuming an average of approximately five ZnS monolayers.[22,96] Data have been averaged over three measurements for each sample. The reported λ_{em} values correspond to the emission peaks from hydrophobic core-shell QDs. [b]Ligand density = ligand number/(QD surface area). [c]FPA = 1/(ligand density).

We now discuss the data on the ligand packing shown in Table 1 within the context of a correlation between the effects of size of the anchoring group (namely the coordination number), the number of PEGylated groups per ligand, and the surface curvature of the QDs. Furthermore, to allow a comparison between our findings and those extracted using alternative analytical techniques, we use three related quantities: the total number of ligands per nanocrystal, ligand density (in nm^{-2}), and footprint area per surface-bound ligand (FPA in nm^2). We find that larger numbers of ligands per nanocrystal are measured for QDs with a larger average surface area (larger radius). This trend is true for all three ligands tested, regardless of their exact architectures. This result is consistent with the expected arrangement of the ligands on the nanocrystals, driven by steric packing, where a larger surface area accommodates more ligands. Conversely, we find that ligands with higher coordination numbers produce a ligand density lower than that of those presenting lower coordination numbers. For example, the density measured for bis(LA)-PEG is approximately 1.5 times lower than that measured for LA-PEG, a result that can be explained by the fact that bis(LA)-PEG with its two anchoring groups occupies more surface area than its mono-LA counterparts. Similarly, the data indicate that the lowest ligand density is measured for LA-$(PEG)_2$, a difference that can be attributed to the bulkier hydrophilic block (two PEG moieties per ligand **L2** vs one moiety for ligand **L1**). Additional insights into the ligand packing on the nanocrystal surfaces can be gained from analysis of the FPA per ligand and its correlation with the QD surface curvature. The FPA value is found to vary with the nanocrystal size for all sets of QDs used (see Figure 6A). Smaller NPs have a larger surface curvature, which yields larger accessible lateral space for each ligand to explore. However, the effects of curvature on the FPA are most pronounced for LA-$(PEG)_2$, where the more bulky hydrophilic blocks can better sample the additional lateral space permitted for smaller nanocrystals (see schematics in Figure 6B). The effects of surface curvature on FPA are less pronounced for the other two ligands: LA-PEG-OCH_3- and bis(LA)-PEG-capped QDs show smaller changes. The increasing coordination number and/or the more pronounced steric effects decrease the number of surface-bound ligands. When the QD size increases, the surface curvature decreases, resulting in a smaller accessible area per ligand (see Figure 6C−D). In that case, the steric hindrance between adjacent PEG chains in the same ligand plays a much larger role than the number of anchoring groups in the ligand packing on the QD surfaces. Overall, the study indicates that a balance between the coordination number and steric effect is crucial for controlling the surface packing density, which is closely linked to the colloidal stability and functionality of NPs.

We stress that the data on the ligand density, extracted using TMSP or/and sodium benzoate as standards, are overall comparable and show similar trends (see Table S1). Nonetheless, data analysis using pyridine as a standard has consistently yielded smaller ligand density values, though the trends for correlating size, surface curvature, and ligand structure are similar to those measured with TMSP and sodium benzoate standards shown above (see Figure S6). Such a difference is attributed to the rather weak coordination binding and/or affinity of pyridine for the unpassivated NP surface.[96] This highlights the importance of selecting the correct external standard for quantitative analyses.

We should note that the major source of errors in estimating the ligand density (and thus the FPA value) derives from uncertainty associated with the measured molar absorption values (ε_{350}) and QD sizes. Uncertainty associated with the size estimate may be larger for smaller size core−shell nanocrystals. These errors will not alter the observed trend in the FPA measured for the various QD−ligand sets described in this study, nonetheless, as those effects will cancel upon comparison of data for different sizes of QDs.

Finally, it is important to draw a direct comparison between the measurements of the ligand arrangement using NMR spectroscopy presented here and previous results reported by our group, in particular those collected using a combination of hydrazone ligation and UV absorption spectroscopy detailed in ref 86. Both approaches are nondisruptive, as hydrazone ligation discussed in our previous study involved small molecule coupling and the appearance of a specific optical feature at 350 nm. However, the ligand density values were extracted from extrapolation to 100% labeling, due to the limited solubility of the hydrazone derivatives. Nonetheless, the measured value for the ligand density and corresponding FPA are remarkably similar for comparably sized QDs. For instance, the ligand FPA measured for the yellow-emitting set of LA-PEG-OCH_3 QDs is ~0.52, while an FPA value of 0.5 was reported for QDs with

DOI: 10.1021/acs.chemmater.8b01033
Chem. Mater. 2018, 30, 3454−3466

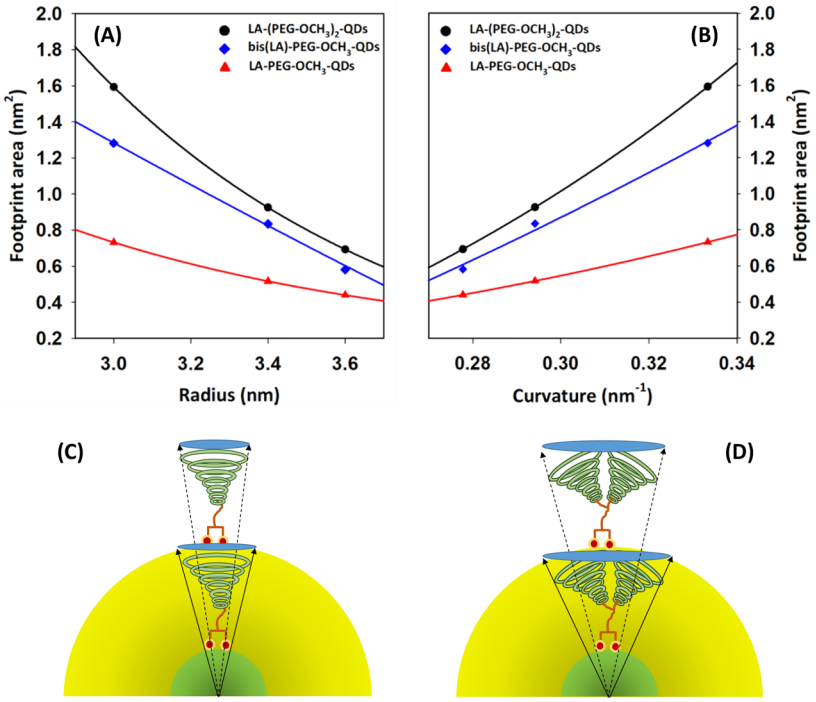

Figure 6. Plots of footprint area (FPA) vs surface QD radius (A) or FPA vs curvature (B) for the nine QD−ligand sets used. The solid lines are added for guidance. (C and D) Schematic model comparing the effect of surface curvature on the footprint area for two different size QDs photoligated with LA-PEG-OCH_3 or with LA-$(PEG\text{-}OCH_3)_2$. The size representation is not to scale and is intended to enhance the effects of the difference in curvature between a small and a larger size nanocrystal.

comparable emission in ref 85. These findings further prove the effectiveness of NMR spectroscopy as a quantitative tool for identifying the structure of the organic capping on various inorganic nanocrystals.

CONCLUSION

We have applied several solution NMR techniques to develop non-invasive characterization of the organic capping layer on hydrophilic CdSe-ZnS QDs. The QDs were rendered biocompatible via photoligation with three sets of lipoic acid-based ligands, containing one or two anchors and one or two PEG chains. We show that by combining the ^1H and DOSY NMR we can identify the sample conditions under which only surface-coordinated ligands are detected. Those data have been supplemented with HSQC measurements, which allowed us to identify when specific overlaps between distinct proton resonances are observed for QD-bound ligands but not for ligands in solution. Estimates of the number of surface ligands are extracted for three different size QDs capped with three distinct sets of ligands (i.e., a total of nine QD−ligand complexes) using the NMR data described above in comparison with those of two internal standards. Three aspects of the coating shell have been discussed, including the total number of ligands per nanocrystal, ligand density, and ligand footprint area. This yielded valuable information correlating the effects of the coordination number, the steric hindrance imposed by the overall size of the PEG blocks, and the surface curvature of the nanocrystal on the solubilizing layer for these materials.

Our results are highly relevant to the use of QDs and other surface-functionalized nanomaterials in biology. They have implications for QD bioconjugation and targeting, imaging, and sensor design based on energy and charge transfer interactions, where the stoichiometry of the conjugates is crucially important. Given the non-invasive nature of NMR spectroscopy, our measurements provide valuable information about the "true" ligand arrangements for these materials. They can easily be extended to other nanocrystals in buffer or hydrophobic media, where information about the molecular arrangements on the QD surfaces is highly valuable.

ASSOCIATED CONTENT

Supporting Information

The Supporting Information is available free of charge on the ACS Publications website at DOI: 10.1021/acs.chemmater.8b01033.

Additional details about QD growth, synthesis of ligands, sample preparation, TEM images, DLS data, along with ^1H NMR, ^{31}P NMR, DOSY NMR, and HSQC data (PDF)

AUTHOR INFORMATION

Corresponding Author

*E-mail: mattoussi@chem.fsu.edu.

ORCID

Birong Zeng: 0000-0003-1582-4929

Hedi Mattoussi: 0000-0002-6511-9323

Present Addresses

§G.P.: Food and Drug Administration, National Center for Toxicological Research, 3900 NCTR Rd., Jefferson, AR 72079.

∥N.Z.: Illumina Corp., 5200 Illumina Way, San Diego, CA 92122.

Notes

The authors declare no competing financial interest.

DOI: 10.1021/acs.chemmater.8b01033
Chem. Mater. 2018, 30, 3454−3466

■ ACKNOWLEDGMENTS

The authors thank the National Science Foundation (NSF-CHE Grants 1508501 and 1058957), the National Institutes of Health (Grant R01 DC013080), and Asahi-Kasei Inc. for financial support and Wentao Wang and Sisi Wang for fruitful discussions.

■ REFERENCES

(1) Gaponenko, S. V. *Optical properties of semiconductor nanocrystals*; Cambridge University Press: Cambridge, U.K., 1998; pp 245.
(2) Klimov, V. I.; Mikhailovsky, A. A.; Xu, S.; Malko, A.; Hollingsworth, J. A.; Leatherdale, C. A.; Eisler, H. J.; Bawendi, M. G. Optical gain and stimulated emission in nanocrystal quantum dots. *Science* **2000**, *290*, 314−317.
(3) Talapin, D. V.; Lee, J. S.; Kovalenko, M. V.; Shevchenko, E. V. Prospects of Colloidal Nanocrystals for Electronic and Optoelectronic Applications. *Chem. Rev.* **2010**, *110*, 389−458.
(4) Klimov, V. I. *Nanocrystal quantum dots*, 2nd ed.; CRC Press: Boca Raton, FL, 2010; pp 469.
(5) Wu, X. Y.; Liu, H. J.; Liu, J. Q.; Haley, K. N.; Treadway, J. A.; Larson, J. P.; Ge, N. F.; Peale, F.; Bruchez, M. P. Immunofluorescent labeling of cancer marker Her2 and other cellular targets with semiconductor quantum dots. *Nat. Biotechnol.* **2003**, *21*, 41−46.
(6) Goldman, E. R.; Clapp, A. R.; Anderson, G. P.; Uyeda, H. T.; Mauro, J. M.; Medintz, I. L.; Mattoussi, H. Multiplexed toxin analysis using four colors of quantum dot fluororeagents. *Anal. Chem.* **2004**, *76*, 684−688.
(7) Sun, Q.; Wang, Y. A.; Li, L. S.; Wang, D.; Zhu, T.; Xu, J.; Yang, C.; Li, Y. Bright, multicoloured light-emitting diodes based on quantum dots. *Nat. Photonics* **2007**, *1*, 717.
(8) Resch-Genger, U.; Grabolle, M.; Cavaliere-Jaricot, S.; Nitschke, R.; Nann, T. Quantum dots versus organic dyes as fluorescent labels. *Nat. Methods* **2008**, *5*, 763−775.
(9) Mattoussi, H.; Palui, G.; Na, H. B. Luminescent quantum dots as platforms for probing in vitro and in vivo biological processes. *Adv. Drug Delivery Rev.* **2012**, *64*, 138−166.
(10) Lee, J.; Sharei, A.; Sim, W. Y.; Adamo, A.; Langer, R.; Jensen, K. F.; Bawendi, M. G. Nonendocytic Delivery of Functional Engineered Nanoparticles into the Cytoplasm of Live Cells Using a Novel, High-Throughput Microfluidic Device. *Nano Lett.* **2012**, *12*, 6322−6327.
(11) Wegner, K. D.; Jin, Z.; Lindén, S.; Jennings, T. L.; Hildebrandt, N. Quantum-Dot-Based Förster Resonance Energy Transfer Immunoassay for Sensitive Clinical Diagnostics of Low-Volume Serum Samples. *ACS Nano* **2013**, *7*, 7411−7419.
(12) Howes, P. D.; Chandrawati, R.; Stevens, M. M. Colloidal nanoparticles as advanced biological sensors. *Science* **2014**, *346*, 1247390.
(13) Lan, X.; Masala, S.; Sargent, E. H. Charge-extraction strategies for colloidal quantum dot photovoltaics. *Nat. Mater.* **2014**, *13*, 233−240.
(14) Silvi, S.; Credi, A. Luminescent sensors based on quantum dot-molecule conjugates. *Chem. Soc. Rev.* **2015**, *44*, 4275−4289.
(15) Kagan, C. R.; Lifshitz, E.; Sargent, E. H.; Talapin, D. V. Building devices from colloidal quantum dots. *Science* **2016**, *353* (6302), aac5523.
(16) Boles, M. A.; Ling, D.; Hyeon, T.; Talapin, D. V. The surface science of nanocrystals. *Nat. Mater.* **2016**, *15*, 141−153.
(17) Bruns, O. T.; Bischof, T. S.; Harris, D. K.; Franke, D.; Shi, Y.; Riedemann, L.; Bartelt, A.; Jaworski, F. B.; Carr, J. A.; Rowlands, C. J.; Wilson, M. W. B.; Chen, O.; Wei, H.; Hwang, G. W.; Montana, D. M.; Coropceanu, I.; Achorn, O. B.; Kloepper, J.; Heeren, J.; So, P. T. C.; Fukumura, D.; Jensen, K. F.; Jain, R. K.; Bawendi, M. G. Next-generation in vivo optical imaging with short-wave infrared quantum dots. *Nat. Biomed. Eng.* **2017**, *1*, 0056.
(18) Hoshino, A.; Fujioka, K.; Oku, T.; Suga, M.; Sasaki, Y. F.; Ohta, T.; Yasuhara, M.; Suzuki, K.; Yamamoto, K. Physicochemical properties and cellular toxicity of nanocrystal quantum dots depend on their surface modification. *Nano Lett.* **2004**, *4*, 2163−2169.
(19) Jeong, S.; Achermann, M.; Nanda, J.; Ivanov, S.; Klimov, V. I.; Hollingsworth, J. A. Effect of the Thiol−Thiolate Equilibrium on the Photophysical Properties of Aqueous CdSe/ZnS Nanocrystal Quantum Dots. *J. Am. Chem. Soc.* **2005**, *127*, 10126−10127.
(20) Green, M. The nature of quantum dot capping ligands. *J. Mater. Chem.* **2010**, *20*, 5797−5809.
(21) Brown, P. R.; Kim, D.; Lunt, R. R.; Zhao, N.; Bawendi, M. G.; Grossman, J. C.; Bulović, V. Energy Level Modification in Lead Sulfide Quantum Dot Thin Films through Ligand Exchange. *ACS Nano* **2014**, *8*, 5863−5872.
(22) Dabbousi, B. O.; RodriguezViejo, J.; Mikulec, F. V.; Heine, J. R.; Mattoussi, H.; Ober, R.; Jensen, K. F.; Bawendi, M. G. (CdSe)ZnS core-shell quantum dots: Synthesis and characterization of a size series of highly luminescent nanocrystallites. *J. Phys. Chem. B* **1997**, *101*, 9463−9475.
(23) Medintz, I.; Uyeda, H.; Goldman, E.; Mattoussi, H. Quantum dot bioconjugates for imaging, labelling and sensing. *Nat. Mater.* **2005**, *4*, 435−446.
(24) Zrazhevskiy, P.; Gao, X. Quantum dot imaging platform for single-cell molecular profiling. *Nat. Commun.* **2013**, *4*, 1619.
(25) Hildebrandt, N.; Spillmann, C. M.; Algar, W. R.; Pons, T.; Stewart, M. H.; Oh, E.; Susumu, K.; Díaz, S. A.; Delehanty, J. B.; Medintz, I. L. Energy Transfer with Semiconductor Quantum Dot Bioconjugates: A Versatile Platform for Biosensing, Energy Harvesting, and Other Developing Applications. *Chem. Rev.* **2017**, *117*, 536−711.
(26) Dubois, F.; Mahler, B.; Dubertret, B.; Doris, E.; Mioskowski, C. A Versatile Strategy for Quantum Dot Ligand Exchange. *J. Am. Chem. Soc.* **2007**, *129*, 482−483.
(27) Dubertret, B.; Skourides, P.; Norris, D. J.; Noireaux, V.; Brivanlou, A. H.; Libchaber, A. In vivo imaging of quantum dots encapsulated in phospholipid micelles. *Science* **2002**, *298*, 1759−1762.
(28) Pellegrino, T.; Manna, L.; Kudera, S.; Liedl, T.; Koktysh, D.; Rogach, A. L.; Keller, S.; Radler, J.; Natile, G.; Parak, W. J. Hydrophobic nanocrystals coated with an amphiphilic polymer shell: A general route to water soluble nanocrystals. *Nano Lett.* **2004**, *4*, 703−707.
(29) Susumu, K.; Uyeda, H. T.; Medintz, I. L.; Pons, T.; Delehanty, J. B.; Mattoussi, H. Enhancing the stability and biological functionalities of quantum dots via compact multifunctional ligands. *J. Am. Chem. Soc.* **2007**, *129*, 13987−13996.
(30) Zylstra, J.; Amey, J.; Miska, N. J.; Pang, L.; Hine, C. R.; Langer, J.; Doyle, R. P.; Maye, M. M. A Modular Phase Transfer and Ligand Exchange Protocol for Quantum Dots. *Langmuir* **2011**, *27*, 4371−4379.
(31) Susumu, K.; Oh, E.; Delehanty, J. B.; Pinaud, F.; Gemmill, K. B.; Walper, S.; Breger, J.; Schroeder, M. J.; Stewart, M. H.; Jain, V.; Whitaker, C. M.; Huston, A. L.; Medintz, I. L. A New Family of Pyridine-Appended Multidentate Polymers As Hydrophilic Surface Ligands for Preparing Stable Biocompatible Quantum Dots. *Chem. Mater.* **2014**, *26*, 5327−5344.
(32) Liu, W. H.; Greytak, A. B.; Lee, J.; Wong, C. R.; Park, J.; Marshall, L. F.; Jiang, W.; Curtin, P. N.; Ting, A. Y.; Nocera, D. G.; Fukumura, D.; Jain, R. K.; Bawendi, M. G. Compact Biocompatible Quantum Dots via RAFT-Mediated Synthesis of Imidazole-Based Random Copolymer Ligand. *J. Am. Chem. Soc.* **2010**, *132*, 472−483.
(33) Palui, G.; Aldeek, F.; Wang, W.; Mattoussi, H. Strategies for interfacing inorganic nanocrystals with biological systems based on polymer-coating. *Chem. Soc. Rev.* **2015**, *44*, 193−227.
(34) Ma, L.; Tu, C.; Le, P.; Chitoor, S.; Lim, S. J.; Zahid, M. U.; Teng, K. W.; Ge, P.; Selvin, P. R.; Smith, A. M. Multidentate Polymer Coatings for Compact and Homogeneous Quantum Dots with Efficient Bioconjugation. *J. Am. Chem. Soc.* **2016**, *138*, 3382−3394.
(35) Schlenoff, J. B. Zwitteration: Coating Surfaces with Zwitterionic Functionality to Reduce Nonspecific Adsorption. *Langmuir* **2014**, *30*, 9625−9636.
(36) Lee, J.; Feng, X.; Chen, O.; Bawendi, M. G.; Huang, J. Stable, small, specific, low-valency quantum dots for single-molecule imaging. *Nanoscale* **2018**, *10*, 4406−4414.

DOI: 10.1021/acs.chemmater.8b01033
Chem. Mater. 2018, 30, 3454−3466

(37) Tasso, M.; Giovanelli, E.; Zala, D.; Bouccara, S.; Fragola, A.; Hanafi, M.; Lenkei, Z.; Pons, T.; Lequeux, N. Sulfobetaine−Vinylimidazole Block Copolymers: A Robust Quantum Dot Surface Chemistry Expanding Bioimaging's Horizons. *ACS Nano* **2015**, *9*, 11479−11489.
(38) Wang, W.; Kapur, A.; Ji, X.; Safi, M.; Palui, G.; Palomo, V.; Dawson, P. E.; Mattoussi, H. Photoligation of an Amphiphilic Polymer with Mixed Coordination Provides Compact and Reactive Quantum Dots. *J. Am. Chem. Soc.* **2015**, *137*, 5438−5451.
(39) Wang, W.; Kapur, A.; Ji, X.; Zeng, B.; Mishra, D.; Mattoussi, H. Multifunctional and High Affinity Polymer Ligand that Provides Bio-Orthogonal Coating of Quantum Dots. *Bioconjugate Chem.* **2016**, *27*, 2024−2036.
(40) Ashraf, S.; Park, J.; Bichelberger, M. A.; Kantner, K.; Hartmann, R.; Maffre, P.; Said, A. H.; Feliu, N.; Lee, J.; Lee, D.; Nienhaus, G. U.; Kim, S.; Parak, W. J. Zwitterionic surface coating of quantum dots reduces protein adsorption and cellular uptake. *Nanoscale* **2016**, *8*, 17794−17800.
(41) Zhan, N.; Palui, G.; Kapur, A.; Palomo, V.; Dawson, P. E.; Mattoussi, H. Controlling the Architecture, Coordination, and Reactivity of Nanoparticle Coating Utilizing an Amino Acid Central Scaffold. *J. Am. Chem. Soc.* **2015**, *137*, 16084−16097.
(42) Wang, W.; Ji, X.; Kapur, A.; Zhang, C.; Mattoussi, H. A Multifunctional Polymer Combining the Imidazole and Zwitterion Motifs as a Biocompatible Compact Coating for Quantum Dots. *J. Am. Chem. Soc.* **2015**, *137*, 14158−14172.
(43) Susumu, K.; Oh, E.; Delehanty, J. B.; Blanco-Canosa, J. B.; Johnson, B. J.; Jain, V.; Hervey, W. J.; Algar, W. R.; Boeneman, K.; Dawson, P. E.; Medintz, I. L. Multifunctional Compact Zwitterionic Ligands for Preparing Robust Biocompatible Semiconductor Quantum Dots and Gold Nanoparticles. *J. Am. Chem. Soc.* **2011**, *133*, 9480−9496.
(44) Liu, D.; Snee, P. T. Water-Soluble Semiconductor Nanocrystals Cap Exchanged with Metalated Ligands. *ACS Nano* **2011**, *5*, 546−550.
(45) Mei, B. C.; Susumu, K.; Medintz, I. L.; Mattoussi, H. Polyethylene glycol-based bidentate ligands to enhance quantum dot and gold nanoparticle stability in biological media. *Nat. Protoc.* **2009**, *4*, 412−423.
(46) Susumu, K.; Mei, B. C.; Mattoussi, H. Multifunctional ligands based on dihydrolipoic acid and polyethylene glycol to promote biocompatibility of quantum dots. *Nat. Protoc.* **2009**, *4*, 424−436.
(47) Mattoussi, H.; Mauro, J. M.; Goldman, E. R.; Anderson, G. P.; Sundar, V. C.; Mikulec, F. V.; Bawendi, M. G. Self-assembly of CdSe-ZnS quantum dot bioconjugates using an engineered recombinant protein. *J. Am. Chem. Soc.* **2000**, *122*, 12142−12150.
(48) Giovanelli, E.; Muro, E.; Sitbon, G.; Hanafi, M.; Pons, T.; Dubertret, B.; Lequeux, N. Highly Enhanced Affinity of Multidentate versus Bidentate Zwitterionic Ligands for Long-Term Quantum Dot Bioimaging. *Langmuir* **2012**, *28*, 15177−15184.
(49) Muro, E.; Pons, T.; Lequeux, N.; Fragola, A.; Sanson, N.; Lenkei, Z.; Dubertret, B. Small and Stable Sulfobetaine Zwitterionic Quantum Dots for Functional Live-Cell Imaging. *J. Am. Chem. Soc.* **2010**, *132* (13), 4556−4557.
(50) Yildiz, I.; McCaughan, B.; Cruickshank, S. F.; Callan, J. F.; Raymo, F. M. Biocompatible CdSe-ZnS Core-Shell Quantum Dots Coated with Hydrophilic Polythiols. *Langmuir* **2009**, *25*, 7090−7096.
(51) Yildiz, I.; Deniz, E.; McCaughan, B.; Cruickshank, S. F.; Callan, J. F.; Raymo, F. M. Hydrophilic CdSe-ZnS Core-Shell Quantum Dots with Reactive Functional Groups on Their Surface. *Langmuir* **2010**, *26*, 11503−11511.
(52) Liu, W.; Howarth, M.; Greytak, A. B.; Zheng, Y.; Nocera, D. G.; Ting, A. Y.; Bawendi, M. G. Compact biocompatible quantum dots functionalized for cellular imaging. *J. Am. Chem. Soc.* **2008**, *130*, 1274−1284.
(53) Rahme, K.; Chen, L.; Hobbs, R. G.; Morris, M. A.; O'Driscoll, C.; Holmes, J. D. PEGylated gold nanoparticles: polymer quantification as a function of PEG lengths and nanoparticle dimensions. *RSC Adv.* **2013**, *3*, 6085−6094.
(54) Benoit, D. N.; Zhu, H.; Lilierose, M. H.; Verm, R. A.; Ali, N.; Morrison, A. N.; Fortner, J. D.; Avendano, C.; Colvin, V. L. Measuring the Grafting Density of Nanoparticles in Solution by Analytical Ultracentrifugation and Total Organic Carbon Analysis. *Anal. Chem.* **2012**, *84*, 9238−9245.
(55) Frederick, M. T.; Achtyl, J. L.; Knowles, K. E.; Weiss, E. A.; Geiger, F. M. Surface-Amplified Ligand Disorder in CdSe Quantum Dots Determined by Electron and Coherent Vibrational Spectroscopies. *J. Am. Chem. Soc.* **2011**, *133*, 7476−7481.
(56) Khitrov, G. A.; Strouse, G. F. ZnS Nanomaterial Characterization by MALDI-TOF Mass Spectrometry. *J. Am. Chem. Soc.* **2003**, *125*, 10465−10469.
(57) Xie, L.; Shen, Y.; Franke, D.; Sebastián, V.; Bawendi, M. G.; Jensen, K. F. Characterization of Indium Phosphide Quantum Dot Growth Intermediates Using MALDI-TOF Mass Spectrometry. *J. Am. Chem. Soc.* **2016**, *138*, 13469−13472.
(58) Wills, A. W.; Kang, M. S.; Khare, A.; Gladfelter, W. L.; Norris, D. J. Thermally Degradable Ligands for Nanocrystals. *ACS Nano* **2010**, *4*, 4523−4530.
(59) Shen, Y.; Roberge, A.; Tan, R.; Gee, M. Y.; Gary, D. C.; Huang, Y.; Blom, D. A.; Benicewicz, B. C.; Cossairt, B. M.; Greytak, A. B. Gel permeation chromatography as a multifunctional processor for nanocrystal purification and on-column ligand exchange chemistry. *Chem. Sci.* **2016**, *7*, 5671−5679.
(60) Wang, M.; Dykstra, T. E.; Lou, X.; Salvador, M. R.; Scholes, G. D.; Winnik, M. A. Colloidal CdSe Nanocrystals Passivated by a Dye-Labeled Multidentate Polymer: Quantitative Analysis by Size-Exclusion Chromatography. *Angew. Chem., Int. Ed.* **2006**, *45*, 2221−2224.
(61) Li, J.; Yang, T.; Chan, W. H.; Choi, M. M. F.; Zhao, D. Synthesis of High-Quality N-Acetyl-l-Cysteine-Capped CdTe Quantum Dots by Hydrothermal Route and the Characterization through MALDI-TOF Mass Spectrometry. *J. Phys. Chem. C* **2013**, *117*, 19175−19181.
(62) Sachleben, J. R.; Colvin, V.; Emsley, L.; Wooten, E. W.; Alivisatos, A. P. Solution-State NMR Studies of the Surface Structure and Dynamics of Semiconductor Nanocrystals. *J. Phys. Chem. B* **1998**, *102*, 10117−10128.
(63) Ribot, F.; Escax, V.; Roiland, C.; Sanchez, C.; Martins, J. C.; Biesemans, M.; Verbruggen, I.; Willem, R. In situ evaluation of interfacial affinity in CeO2 based hybrid nanoparticles by pulsed field gradient NMR. *Chem. Commun.* **2005**, 1019−1021.
(64) Moreels, I.; Fritzinger, B.; Martins, J. C.; Hens, Z. Surface Chemistry of Colloidal PbSe Nanocrystals. *J. Am. Chem. Soc.* **2008**, *130*, 15081−15086.
(65) Virieux, H.; Le Troedec, M.; Cros-Gagneux, A.; Ojo, W.-S.; Delpech, F.; Nayral, C.; Martinez, H.; Chaudret, B. InP/ZnS Nanocrystals: Coupling NMR and XPS for Fine Surface and Interface Description. *J. Am. Chem. Soc.* **2012**, *134*, 19701−19708.
(66) Cros-Gagneux, A.; Delpech, F.; Nayral, C.; Cornejo, A.; Coppel, Y.; Chaudret, B. Surface Chemistry of InP Quantum Dots: A Comprehensive Study. *J. Am. Chem. Soc.* **2010**, *132*, 18147−18157.
(67) Morris-Cohen, A. J.; Malicki, M.; Peterson, M. D.; Slavin, J. W. J.; Weiss, E. A. Chemical, Structural, and Quantitative Analysis of the Ligand Shells of Colloidal Quantum Dots. *Chem. Mater.* **2013**, *25*, 1155−1165.
(68) Knittel, F.; Gravel, E.; Cassette, E.; Pons, T.; Pillon, F.; Dubertret, B.; Doris, E. On the Characterization of the Surface Chemistry of Quantum Dots. *Nano Lett.* **2013**, *13*, 5075−5078.
(69) Shen, Y.; Gee, M. Y.; Tan, R.; Pellechia, P. J.; Greytak, A. B. Purification of Quantum Dots by Gel Permeation Chromatography and the Effect of Excess Ligands on Shell Growth and Ligand Exchange. *Chem. Mater.* **2013**, *25*, 2838−2848.
(70) Smith, A. M.; Johnston, K. A.; Crawford, S. E.; Marbella, L. E.; Millstone, J. E. Ligand density quantification on colloidal inorganic nanoparticles. *Analyst* **2017**, *142*, 11−29.
(71) Smith, A. M.; Marbella, L. E.; Johnston, K. A.; Hartmann, M. J.; Crawford, S. E.; Kozycz, L. M.; Seferos, D. S.; Millstone, J. E. Quantitative Analysis of Thiolated Ligand Exchange on Gold

DOI: 10.1021/acs.chemmater.8b01033
Chem. Mater. 2018, 30, 3454−3466

Nanoparticles Monitored by 1H NMR Spectroscopy. *Anal. Chem.* **2015**, *87*, 2771−2778.
(72) Al-Johani, H.; Abou-Hamad, E.; Jedidi, A.; Widdifield, C. M.; Viger-Gravel, J.; Sangaru, S. S.; Gajan, D.; Anjum, D. H.; Ould-Chikh, S.; Hedhili, M. N.; Gurinov, A.; Kelly, M. J.; El Eter, M.; Cavallo, L.; Emsley, L.; Basset, J.-M. The structure and binding mode of citrate in the stabilization of gold nanoparticles. *Nat. Chem.* **2017**, *9*, 890.
(73) Anderson, N. C.; Owen, J. S. Soluble, Chloride-Terminated CdSe Nanocrystals: Ligand Exchange Monitored by 1H and 31P NMR Spectroscopy. *Chem. Mater.* **2013**, *25*, 69−76.
(74) Hens, Z.; Martins, J. C. A Solution NMR Toolbox for Characterizing the Surface Chemistry of Colloidal Nanocrystals. *Chem. Mater.* **2013**, *25*, 1211−1221.
(75) Gomes, R.; Hassinen, A.; Szczygiel, A.; Zhao, Q.; Vantomme, A.; Martins, J. C.; Hens, Z. Binding of Phosphonic Acids to CdSe Quantum Dots: A Solution NMR Study. *J. Phys. Chem. Lett.* **2011**, *2*, 145−152.
(76) Donakowski, M. D.; Godbe, J. M.; Sknepnek, R.; Knowles, K. E.; Olvera de la Cruz, M.; Weiss, E. A. A Quantitative Description of the Binding Equilibria of para-Substituted Aniline Ligands and CdSe Quantum Dots. *J. Phys. Chem. C* **2010**, *114*, 22526−22534.
(77) Tamang, S.; Beaune, G.; Texier, I.; Reiss, P. Aqueous Phase Transfer of InP/ZnS Nanocrystals Conserving Fluorescence and High Colloidal Stability. *ACS Nano* **2011**, *5*, 9392−9402.
(78) De Roo, J.; Coucke, S.; Rijckaert, H.; De Keukeleere, K.; Sinnaeve, D.; Hens, Z.; Martins, J. C.; Van Driessche, I. Amino Acid-Based Stabilization of Oxide Nanocrystals in Polar Media: From Insight in Ligand Exchange to Solution 1H NMR Probing of Short-Chained Adsorbates. *Langmuir* **2016**, *32*, 1962−1970.
(79) Peng, Z. A.; Peng, X. Formation of High-Quality CdTe, CdSe, and CdS Nanocrystals Using CdO as Precursor. *J. Am. Chem. Soc.* **2001**, *123*, 183−184.
(80) Clapp, A. R.; Goldman, E. R.; Mattoussi, H. Capping of CdSe-ZnS quantum dots with DHLA and subsequent conjugation with proteins. *Nat. Protoc.* **2006**, *1*, 1258−1266.
(81) Murray, C. B.; Norris, D. J.; Bawendi, M. G. Synthesis and Characterization of Nearly Monodisperse Cde (E = S, Se, Te) Semiconductor Nanocrystallites. *J. Am. Chem. Soc.* **1993**, *115*, 8706−8715.
(82) Peng, X. G.; Schlamp, M. C.; Kadavanich, A. V.; Alivisatos, A. P. Epitaxial growth of highly luminescent CdSe/CdS core/shell nanocrystals with photostability and electronic accessibility. *J. Am. Chem. Soc.* **1997**, *119*, 7019−7029.
(83) Uyeda, H. T.; Medintz, I. L.; Jaiswal, J. K.; Simon, S. M.; Mattoussi, H. Synthesis of compact multidentate ligands to prepare stable hydrophilic quantum dot fluorophores. *J. Am. Chem. Soc.* **2005**, *127*, 3870−3878.
(84) Palui, G.; Avellini, T.; Zhan, N.; Pan, F.; Gray, D.; Alabugin, I.; Mattoussi, H. Photoinduced Phase Transfer of Luminescent Quantum Dots to Polar and Aqueous Media. *J. Am. Chem. Soc.* **2012**, *134*, 16370−16378.
(85) Oh, E.; Susumu, K.; Blanco-Canosa, J. B.; Medintz, I. L.; Dawson, P. E.; Mattoussi, H. Preparation of Stable Maleimide-Functionalized Au Nanoparticles and Their Use in Counting Surface Ligands. *Small* **2010**, *6*, 1273−1278.
(86) Zhan, N.; Palui, G.; Merkl, J.-P.; Mattoussi, H. Bio-orthogonal Coupling as a Means of Quantifying the Ligand Density on Hydrophilic Quantum Dots. *J. Am. Chem. Soc.* **2016**, *138*, 3190−3201.
(87) De Nolf, K.; Cosseddu, S. M.; Jasieniak, J. J.; Drijvers, E.; Martins, J. C.; Infante, I.; Hens, Z. Binding and Packing in Two-Component Colloidal Quantum Dot Ligand Shells: Linear versus Branched Carboxylates. *J. Am. Chem. Soc.* **2017**, *139*, 3456−3464.
(88) Chen, P. E.; Anderson, N. C.; Norman, Z. M.; Owen, J. S. Tight Binding of Carboxylate, Phosphonate, and Carbamate Anions to Stoichiometric CdSe Nanocrystals. *J. Am. Chem. Soc.* **2017**, *139*, 3227−3236.
(89) Morris-Cohen, A. J.; Donakowski, M. D.; Knowles, K. E.; Weiss, E. A. The Effect of a Common Purification Procedure on the Chemical Composition of the Surfaces of CdSe Quantum Dots Synthesized with Trioctylphosphine Oxide. *J. Phys. Chem. C* **2010**, *114*, 897−906.
(90) Zeng, B.; Palui, G.; Zhang, C.; Zhan, N.; Wang, W.; Ji, X.; Chen, B.; Mattoussi, H. Characterization of the Ligand Capping of Hydrophobic CdSe−ZnS Quantum Dots Using NMR Spectroscopy. *Chem. Mater.* **2018**, *30*, 225−238.
(91) Morris, K. F.; Johnson, C. S. Diffusion-ordered two-dimensional nuclear magnetic resonance spectroscopy. *J. Am. Chem. Soc.* **1992**, *114*, 3139−3141.
(92) Novoa-Carballal, R.; Fernandez-Megia, E.; Jimenez, C.; Riguera, R. NMR methods for unravelling the spectra of complex mixtures. *Nat. Prod. Rep.* **2011**, *28*, 78−98.
(93) Claridge, T. D. W. Chapter 2: Introducing High-Resolution NMR. In *High-Resolution NMR Techniques in Organic Chemistry*, 3rd ed.; Elsevier: Boston, 2016; pp 11−59.
(94) Wehrli, F. W.; Wirthlin, T. *Interpretation of Carbon-13 NMR Spectra*; Heyden, 1976.
(95) Leatherdale, C. A.; Woo, W. K.; Mikulec, F. V.; Bawendi, M. G. On the absorption cross section of CdSe nanocrystal quantum dots. *J. Phys. Chem. B* **2002**, *106*, 7619−7622.
(96) Mattoussi, H.; Cumming, A. W.; Murray, C. B.; Bawendi, M. G.; Ober, R. Properties of CdSe nanocrystal dispersions in the dilute regime: Structure and interparticle interactions. *Phys. Rev. B: Condens. Matter Mater. Phys.* **1998**, *58*, 7850−7863.

DOI: 10.1021/acs.chemmater.8b01033
Chem. Mater. 2018, 30, 3454−3466